Towards a Better Understanding of Deep Neural Networks Representations using Deep Generative Networks

Jérémie Despraz[1,2], Stéphane Gomez[1,2], Héctor F. Satizábal[1] and Carlos Andrés Peña-Reyes[1,2]
[1]*School of Business and Engineering Vaud (HEIG-VD), University of Applied Sciences of Western Switzerland (HES-SO), Yverdon-les-Bains, Switzerland*
[2]*Computational Intelligence for Computational Biology (CI4CB), SIB Swiss Institute of Bioinformatics, Lausanne, Switzerland*

Keywords: Deep-Learning, Convolutional Neural Networks, Generative Neural Networks, Activation Maximization, Interpretability.

Abstract: This paper presents a novel approach to deep-dream-like image generation for convolutional neural networks (CNNs). Images are produced by a deep generative network from a smaller dimensional feature vector. This method allows for the generation of more realistic looking images than traditional activation-maximization methods and gives insight into the CNN's internal representations. Training is achieved by standard backpropagation algorithms.

1 INTRODUCTION

Artificial deep-neural networks have proven extremely successful in a wide variety of tasks but remain extremely opaque in terms of what they learn and how they use their acquired knowledge to make predictions. In particular, without any insight into the network, the task of determining whether it has properly integrated a specific concept is very difficult and the subsequent validation of the method for critical activities is not possible. Furthermore, without a tool to interrogate the network concerning what it has learned from a given dataset, it is very difficult to transfer the acquired knowledge from the network parameters to a human user. These considerations demonstrate the need for methods that would allow us to gain better insight into deep-neural networks.

This paper makes a step in that direction with the introduction of a method that can produce preferred inputs to a trained network, thus enabling the creation of representative and interpretable data that reflects the network's internal representations.

2 RELATED WORK

Extensive work has been recently done towards better understanding artificial neural networks, especially in the domain of convolutional neural networks (CNN). In particular, several methods have been proposed in order to gain insight into the internal representations and decision-making processes of the neural networks. Yosinski et al. (Yosinski et al., 2015) developed a tool to visualize filter activation given an input image. They also introduced a method for gradient ascent that modifies each single pixel of the input as to maximize a given neuron activation, resulting in human interpretable but fairly unrealistic-looking images of preferred inputs (see Figure 1). Other researchers have developed methods to highlight specific regions of interest of an input image. Springenberg et al. (Springenberg et al., 2014) introduced guided-backpropagation, a modified implementation of the standard backpropagation method, that emphasizes parts of the image connected to a given class by a sequence of strictly positive weights. Zeiler et al. (Zeiler and Fergus, 2014) also introduced a novel visualization technique based on deconvolution and filter activation. Simonyan et al. (Simonyan et al., 2013) used gradient backpropagation on the original network input to compute saliency maps and to extract relevant features from images.

A more recent approach that has been very successful at creating patterns closely matching the properties of real images are generative methods. This field is very dynamic and methods have evolved quickly, from the generation of images by evolution-

Despraz J., Gomez S., SatizÃąbal H. and PeÃśa-Reyes C.
Towards a Better Understanding of Deep Neural Networks Representations using Deep Generative Networks.
DOI: 10.5220/0006495102150222
In *Proceedings of the 9th International Joint Conference on Computational Intelligence (IJCCI 2017)*, pages 215-222
ISBN: 978-989-758-274-5

ary algorithms using direct and indirect encodings (Nguyen et al., 2015), to more complex reconstruction techniques (Mahendran and Vedaldi, 2015), to the current state-of-the-art generative adversarial networks (GANs) (Radford et al., 2015).

Studies on GANs have demonstrated that deep-generative networks can be used to create images exhibiting properties very similar to natural ones, sometimes making them indistinguishable to humans (Denton et al., 2015). In this context, other researchers have developed methods capable of generating preferred inputs for activation maximization. In particular, a method similar to the one presented herein has been recently proposed by Nguyen et al. (Nguyen et al., 2016) that allows generating photo-realistic images from a deep-generative neural network. In order to obtain well-structured images, they used part of a GAN network, previously trained, to generate sets of images similar to the ones they targeted. To ensure the convergence of the optimization to a realistic-looking image, they further constrained the inputs to be within a well defined range, allowing only for values that trigger neuron responses close to the ones measured with images from the train dataset. It is only upon our own work's completion that we became aware of such a closely-related work, carried out in parallel to ours. While we have chosen similar approaches, some points differ. In particular, our implementation used less restrictive constraints on the parameters and considered configurations where the network's weights were randomly initialized and optimized. Also, we implemented our method on top of the very deep VGG-16 model (Simonyan and Zisserman, 2014), a model that was not considered in the aforementioned study.

Details on our specific implementation are presented in Section 3.

3 METHODS

The core idea of the proposed method is to couple a generative deep-neural network (G) to a pretrained CNN (D) as depicted schematically on Figure 2. The weights of the classifier D are assumed to be already optimized for a specific classification task and remain fixed. The activation functions are also kept, except for the last classification layer where the usual softmax functions are replaced with rectified linear units (ReLUs).

The resulting coupled network has one input layer: a 1-dimensional feature vector, and two output layers: an image whose dimensions are identical to D's inputs and a series of activations for each out-

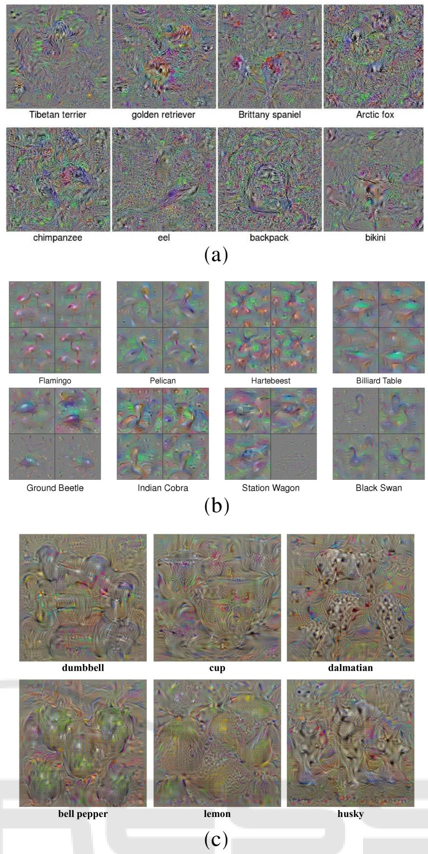

Figure 1: Examples from previous works showing preferred input images constructed by activation maximization methods that do not rely on a deep generative network. (Images (a), (b), and (c) from (Nguyen et al., 2015; Yosinski et al., 2015; Simonyan et al., 2013), respectively).

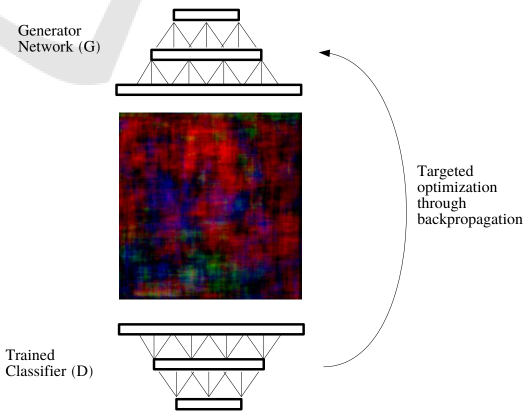

Figure 2: Architecture of a coupled generative-discriminative network. The generative network G creates images from an input feature vector and these images are fed to the already-trained discriminator D. The weights of D are fixed and the entire coupled network is trained with a specific loss function so as to make G generate images that yield the desire response from D.

put neuron of D. The task of G is to generate an image that maximizes the activation of a particular output neuron of D:

$$\text{feature space} \underset{G}{\longrightarrow} \text{image} \underset{D}{\longrightarrow} \text{class-neuron activation}$$

The transformation from feature space to image space is a mapping from $\mathbb{R}^m$ to $\mathbb{R}^{n \times n}$, and is achieved through a series of upsampling, convolution, and batch normalization operations. The feature vector $\mathbf{f}$ is built as:

$$(f_1, \ldots, f_m)^T = \left(\alpha_1 \varepsilon(f_1^{(0)}), \ldots, \alpha_m \varepsilon(f_m^{(0)})\right)^T \quad (1)$$

where the expression $\varepsilon(\cdot)$ is a function introducing a random Gaussian perturbation (similar to jitter in other works (Mahendran and Vedaldi, 2016)), $f_i^{(0)} \in \mathbb{R}$ are constant parameters, and $\alpha_i \in \mathbb{R}$ are parameters to be optimized.

In order to generate an image that maximizes the expression of a single target class c_i, we define the loss function of our coupled network as:

$$loss = -a(c_i) + \lambda \sum_{i \neq j} a(c_j) + R(\xi) \quad (2)$$

where $a(\cdot)$ is the target neuron activation function, $\lambda \in \mathbb{R}_+$ is a factor penalizing the activation of other classes, and $R(\xi)$ is a regularizer defined on a subset of parameters ξ of the generator network.

The loss function is then minimized using standard backpropagation methods over the entire coupled network. The choice of ReLU as the activation function on the last layer is justified because it prevents a decrease in the loss function due to negative contributions of non-targeted neurons c_j. Therefore, in the case where $a(c_j) = 0 \ \forall j \neq i$ (i.e. all classes other than i do not contribute to the loss), the optimization should favor a maximal expression of the target neuron c_i. Convergence can be controlled by ensuring that $a(c_i) > 0 \ \forall t$ thus removing the risk of having $d(loss) = 0$ at some point in the optimization which would prevent full convergence to the optimum solution.

We considered two distinct approaches for the construction of network G. One where we initialize each layer with random weights and biases, and one where we extract G from a trained denoising autoencoder (Vincent et al., 2010) as illustrated in Figure 3. The advantage of the second method is that the network G has already learned a mapping from the input feature vector space to a set of natural images. Therefore, the optimization problem is reduced to the task of finding coordinates of the feature vector that yield the strongest activation of the target neuron.

Table 1 lists the parameters and optimizers used for training. The detailed network architecture can be found in the Appendix.

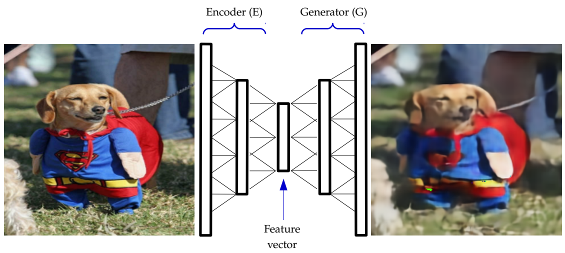

Figure 3: Architecture of the denoising autoencoder (Vincent et al., 2010). It is composed of an encoder network (E) that generates a feature vector representation from the noisy input image and a generative network (G) that attempts to regenerate the original image from the feature vector.

Table 1: Implementation details and parameters used for optimization of the coupled deep-networks in the untrained and pretrained configurations.

	No pretraining	With pretraining
Variables	5.240.841	3.200
Optimizer	AdaMax (Kingma and Ba, 2014)	Stochastic gradient descent
Parameters	learning rate = 0.002, $\beta_1 = 0.9$, $\beta_2 = 0.999$, decay = 0, $\varepsilon = 10^{-08}$	learning rate = 0.01, momentum = 0.1, Nesterov momentum, decay = 0
Initial conditions	$\mathbf{f} = \mathbf{1}$	$\mathbf{f} = \mathbf{0}$
Noise parameters	type = additive, $\mu = 0$, $\sigma = 2$	type = multiplicative, $\mu = 1$, $\sigma = 0.05$

It is worth noting that this method is not limited to class description as it can be applied identically to any neuron or group of neuron activations in the CNN by simply adapting the loss function in Equation 2. As a result, it allows the generation of images representing arbitrary-level (low, mid, or high) features learned by a CNN as well as any combination of them.

4 RESULTS

In order to test our method, we used the freely available, very deep VGG-16 model (Simonyan and Zisserman, 2014) as a target discriminator and we constructed a generator whose full architecture is described by Table 2 in the Appendix. To implement, test, and optimize the deep-neural networks, we used the open-source library Keras (Chollet, 2015) with the Tensorflow (Abadi et al., 2016) backend. Sections 4.1 and 4.2 present the results obtained by optimizing the loss function for network G as defined by Equation 2, without and with pretraining, respectively.

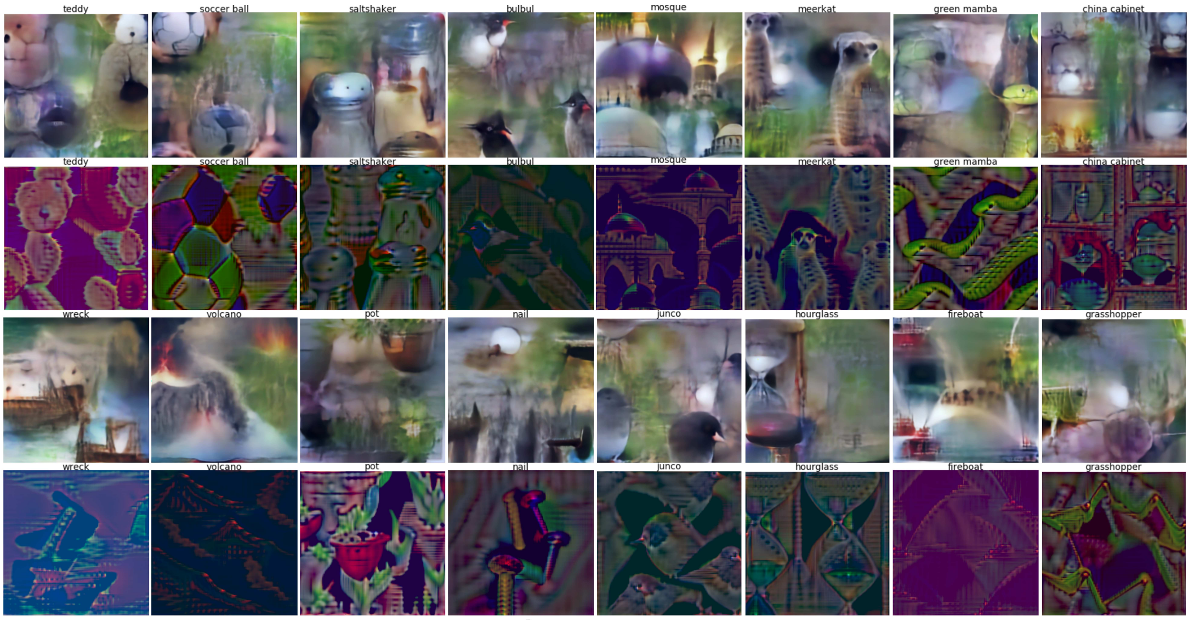

Figure 4: Selection of images generated by both methods (lines 1 and 3 are outputs of the pretrained network). Each row contains two couples of images sharing the same target class label. Images created with the pretrained network are less saturated, and often possess a more complex spatial structure making them visually more resemblant to natural images. This image is best viewed in color/screen.

4.1 Without Pretraining

In this setup, the regularizer expression of Equation 2 becomes:

$$R(\xi) = 0.01\ell_1(\gamma) = 0.01\sum_{k=1}^{3}|\gamma_k| \qquad (3)$$

where γ_k are the weights associated with the 3 channels of the generated image. This expression prevents the possible drift toward over-saturated images. A few examples of generated images are presented in Figure 4.

Images generated with this method can be, for the most part, easily interpreted by a human, as the main features of the class generally appear quite clearly. It is also worth noting that the network is capable of creating a wide variety of shapes and textures that are close to those seen on natural images, despite the fact that it has never "seen" an actual image and therefore has no preexisting internal representations of these features.

However, these images also often display unrealistic colors as well as low spatial ordering. Most of the time, we observed typical class patterns that are repeated over the entire image. This is probably partly due to the fairly large amount of noise that is generated on the feature vector that has been deemed necessary to ensure convergence to a visually interesting solution. These issues are, in part, tackled by introducing pretraining.

4.2 With Pretraining

We used a dataset of dog pictures from ImageNet (Russakovsky et al., 2015) to train the denoising autoencoder illustrated in Figure 3. The advantage of the dog dataset with respect to some other classes of ImageNet is the variety of pictures it contains. It comprises for instance many subclasses corresponding to several different dog breeds, each with its special attributes (color, shape, fur type, size, etc.) taken in various contexts and locations. This allowed the autoencoder to be exposed to a wide variety of images, thus reinforcing its ability to reconstruct the different features present in the VGG-16 classes.

Before feeding the images to the network, Gaussian noise was added to improve the quality of the learning process (Vincent et al., 2010) and error was measured as the mean-squared Euclidian distance between the input and the reconstructed image. This approach is relatively light and easy to implement. However, it has the disadvantage of leading the generator G to produce blurry images, cutting off some high frequency components of the original input. In this configuration, the regularizer expression from Equation 2 becomes:

$$R(\xi) = 0.1\ell_2(\alpha) = 0.1\sqrt{\sum_{k=1}^{N}\alpha_k^2} \qquad (4)$$

where α_k are the weights of the first layer (see Equation 1) and N is the length of the input feature vector.

This expression keeps the coordinates of the feature vector in a reasonable range. Furthermore, we assume that the network has learned a good-enough mapping from the feature space to the real-image space. Thus, with the exception of the first layer, we fix the weights of the entire autoencoder, hence dramatically reducing the amount of parameters to be trained. A few examples of generated images are presented in Figure 4.

Interestingly, images produced with this setup have much more realistic colors and seem to have a greater level of structure with respect to the implementation shown in Section 4.1. For many of the generated pictures, a posteriori class identification can be done without too much effort. Also, the network is able to reproduce patterns that have not been previously "seen" (and therefore, that could not have been learned a priori) as it was trained exclusively with pictures belonging to the *dog* class.

However, it also appears that the network is not able to reproduce sharp details and has trouble reproducing high frequency components observed in natural images. This limitation is most probably linked to the pretraining phase of the autoencoder where the choice of RMSE as loss function did not account enough for high frequency terms.

A comparison of our method with (Nguyen et al., 2016) (see Figure 5), suggests that our results might be improved further, for instance by using a generative network previously trained to reproduce highly realistic images. While the level of details provided by our method is not as high as in Nguyen's, we observe similar features on the generated images of a given class.
The original code as well as images for all the 1,000 classes of the VGG-16 network were generated with both of the presented methods and are available for download at https://github.com/jdespraz/deep_generative_networks.

5 DISCUSSION AND APPLICATIONS

As we have seen, the method introduced in this paper allows the generation of images that have a structure similar to natural images. This represents a great advantage with respect to most generative techniques, such as deep-dreams and other input-based optimizations methods (see Figures 1 and Figure 4 for comparison). Also, since it does not require any modifications or re-optimization of the discriminative network (as in GANs for example), the method does not alter the original network and can be applied effectively directly by coupling a generative network and using standard backpropagation algorithms. The implementation is therefore relatively simple and not excessively costly in terms of computation time.

Figure 5: Comparison with (Nguyen et al., 2016) (left column) and our method (right column) for the classes Mosque, Candle, Leaf Beatle, and Lawn Mower.

In addition, our method enables various new techniques of deep-neural network analysis that we present in this section.

5.1 Interpretability

The analysis of the generated images allows for some degree of interpretation of the discriminator network's internal representation of the classes. In particular, it appears that some classes have been trained with biased samples, and this bias is reflected in the generated images. Typical examples are presented in Figures 6 and 7. Interestingly, it seems that the bias is more strongly expressed with the pretrained network.

We observe for example that the classes *crib* and *cradle* both lead the network to generate images of a baby, the *miniskirt* class seems to react to naked legs, and *muzzle* includes information about dogs' faces.
Similarly, for musical instruments, as illustrated in Figure 7 by the *harmonica* class, they appear most of the time in the training set held by musicians and, as a result, the network seems to include in these classes the arms and fingers as if they were part of the object. The same can be observed with the class *tench* where images in the train dataset contain many instances of fishermen holding the fish in their hands and generated images do therefore include properties of the fish

Figure 6: First selection of images displaying some bias in the network's internal representations. Row 1 shows the outcome of the pretrained network, row 2 the untrained network, and row 3 a typical example of the training dataset. Biases seem to appear more clearly in the outputs of the trained network.

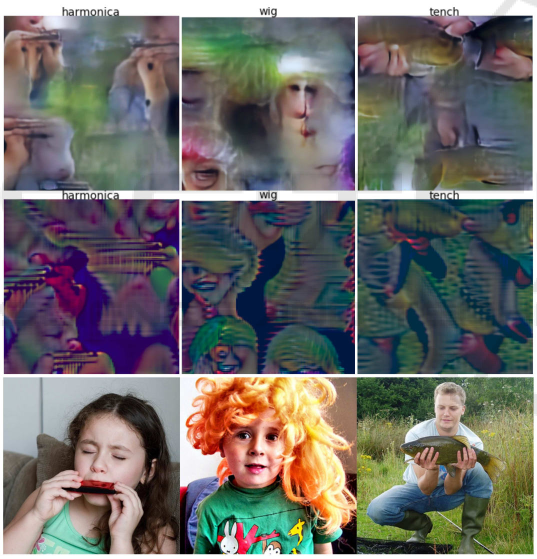

Figure 7: Second selection of images displaying some bias in the network's internal representations. Row 1 shows the outcome of the pretrained network, row 2 the untrained network and row 3 a typical example of the train dataset. Biases seem to appear more clearly in the outputs of the trained network.

as well as human fingers.

Being able to interpret the network's acquired knowledge in such a way is extremely useful as it allows us to improve the quality of the training by detecting and removing observed biases, leading eventually to more robust, accurate, and reliable predictions.

5.2 Knowledge Discovery

This method can potentially be used to gather new (possibly unknown) information about the training data. For example, let us assume the scenario where a deep-neural network has been trained to detect and classify patients with lung cancer based on radiographic images, classifying them into two classes, "ill" or "healthy". If we were to generate images that strongly activate the "ill" class of this network, we could have an idea of the signs the network has learned to recognize cancerous cells, potentially discovering new features of cancer images.

5.3 Feature Explanation

In the domain of rule or feature extraction, one tries to extract knowledge from deep-neural networks in order to better explain their behavior. With CNNs, the extracted information is sometimes represented in the form of rules consisting of a set of weighted filter indices. While these rules may accurately reflect the network's behavior, they are often difficult to understand; filters are often not easily interpretable and their linear combinations can be even more obscure. In this context, our method could allow the generation of images displaying a graphical representation of a set of extracted filters, thus allowing for a more easily interpretable explanation rather than having a simple set of feature identifiers. This could easily be achieved simply by replacing the activation of neuron c_i in Equation 2 by a group of neurons corresponding to a set of features.

Figure 8 illustrates some of the representations obtained for a set of filters on two different network layers. It clearly highlights the hierarchical structure of the network since filters close to the input react strongly to simple patterns whereas filters closer to the output display much more complex structures. Some of these high-level features are also easily recognizable as for instance ears, eyes, hands or clothes.

5.4 Generative Tools

Another usage of this method can be the generation of compound images, containing features of several classes. Some examples of such images are presented in Figure 9 where we constructed images that maximize the output of two distinct classes. Generated images display attributes of the two classes, and these characteristics are sometimes present in the texture (such as the jigsaw puzzle) or mixed in a single object (such as with the ostrich and the bullfrog).

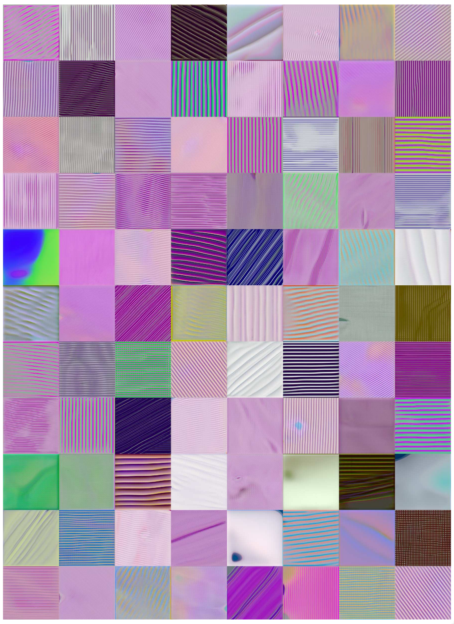

(a) Generated images for filters of the 9th layer

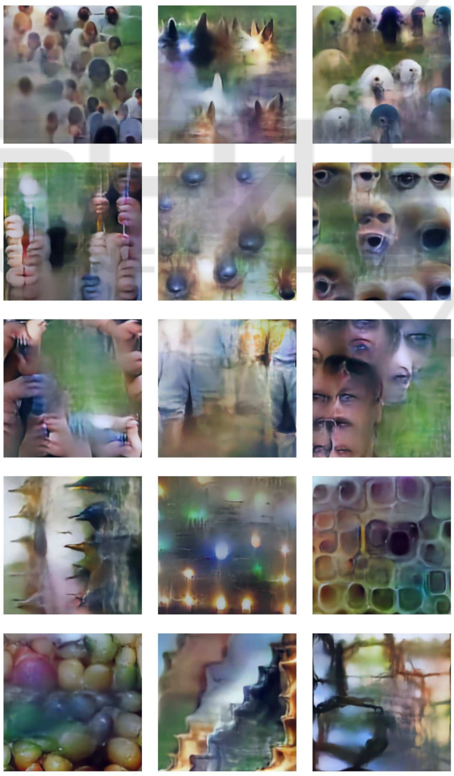

(b) Generated images for filters of the 26th layer

Figure 8: Selection of generated images that maximize filter responses of a given network layer. As expected, preferred images for layers close to the input exhibit simple patterns (straight lines, uniform colors) and the complexity of these patterns increases as we get deeper into the network. Some of the high-level features such as eyes, hands, ears or dog's faces can easily be recognized.

Figure 9: Some examples of images generated to maximize the activation of two classes. Resulting images display attributes of both classes.

We can imagine a wide variety of applications for a tool capable of mixing various image attributes, from a pure artistic perspective of creating new content to a more pragmatic approach of generating preferred inputs for specific CNN layers or filters. In particular, it would be very interesting to couple this approach with a feature selection tool that would generate images corresponding to a particularly relevant feature or a combination of those. Besides, several methods of feature extraction have already been successfully developed and implemented (Ribeiro et al., 2016; Zhou et al., 2015).

6 CONCLUSION

We have presented a method that allows the generation of images that trigger a strong response of a target neuron in a trained classifier. We have considered an approach where the generative network is trained from scratch, and another where it was first trained to generate natural images from a lower dimensional feature vector.

The resulting images display some degree of structure and detail that is similar to real images and allows interpretations of the network's internal representations. We have demonstrated that complex levels of structure and patterns can be generated without ever being "seen" by a deep-neural network, simply by minimizing a well chosen loss function.

Finally, we presented potential applications of this method in neural network interpretation, data analysis and image generation. In particular, we have demonstrated through examples the usefulness of such an approach to detect biases in the network's internal representations.

ACKNOWLEDGEMENTS

This work was supported by the Hasler Fundation, project number 16015.

REFERENCES

Abadi, M., Agarwal, A., Barham, P., Brevdo, E., Chen, Z., Citro, C., Corrado, G. S., Davis, A., Dean, J., Devin, M., et al. (2016). Tensorflow: Large-scale machine learning on heterogeneous distributed systems. *arXiv preprint arXiv:1603.04467*.

Chollet, F. (2015). Keras.

Denton, E. L., Chintala, S., Fergus, R., et al. (2015). Deep generative image models using a laplacian pyramid of adversarial networks. In *Advances in neural information processing systems*, pages 1486–1494.

Kingma, D. and Ba, J. (2014). Adam: A method for stochastic optimization. *arXiv preprint arXiv:1412.6980*.

Mahendran, A. and Vedaldi, A. (2015). Understanding deep image representations by inverting them. In *2015 IEEE conference on computer vision and pattern recognition (CVPR)*, pages 5188–5196. IEEE.

Mahendran, A. and Vedaldi, A. (2016). Visualizing deep convolutional neural networks using natural pre-images. *International Journal of Computer Vision*, 120(3):233–255.

Nguyen, A., Dosovitskiy, A., Yosinski, J., Brox, T., and Clune, J. (2016). Synthesizing the preferred inputs for neurons in neural networks via deep generator networks. In *Advances in Neural Information Processing Systems*, pages 3387–3395.

Nguyen, A., Yosinski, J., and Clune, J. (2015). Deep neural networks are easily fooled: High confidence predictions for unrecognizable images. In *2015 IEEE Conference on Computer Vision and Pattern Recognition (CVPR)*, pages 427–436. IEEE.

Radford, A., Metz, L., and Chintala, S. (2015). Unsupervised representation learning with deep convolutional generative adversarial networks. *arXiv preprint arXiv:1511.06434*.

Ribeiro, M. T., Singh, S., and Guestrin, C. (2016). " why should i trust you?": Explaining the predictions of any classifier. *arXiv preprint arXiv:1602.04938*.

Russakovsky, O., Deng, J., Su, H., Krause, J., Satheesh, S., Ma, S., Huang, Z., Karpathy, A., Khosla, A., Bernstein, M., et al. (2015). Imagenet large scale visual recognition challenge. *International Journal of Computer Vision*, 115(3):211–252.

Simonyan, K., Vedaldi, A., and Zisserman, A. (2013). Deep inside convolutional networks: Visualising image classification models and saliency maps. *arXiv preprint arXiv:1312.6034*.

Simonyan, K. and Zisserman, A. (2014). Very deep convolutional networks for large-scale image recognition. *arXiv preprint arXiv:1409.1556*.

Springenberg, J. T., Dosovitskiy, A., Brox, T., and Riedmiller, M. (2014). Striving for simplicity: The all convolutional net. *arXiv preprint arXiv:1412.6806*.

Vincent, P., Larochelle, H., Lajoie, I., Bengio, Y., and Manzagol, P.-A. (2010). Stacked denoising autoencoders: Learning useful representations in a deep network with a local denoising criterion. *Journal of Machine Learning Research*, 11(Dec):3371–3408.

Yosinski, J., Clune, J., Nguyen, A., Fuchs, T., and Lipson, H. (2015). Understanding neural networks through deep visualization. *arXiv preprint arXiv:1506.06579*.

Zeiler, M. D. and Fergus, R. (2014). Visualizing and understanding convolutional networks. In *European Conference on Computer Vision*, pages 818–833. Springer.

Zhou, B., Khosla, A., Lapedriza, A., Oliva, A., and Torralba, A. (2015). Learning deep features for discriminative localization. *arXiv preprint arXiv:1512.04150*.

APPENDIX

The network detailed architecture is presented in this section. You can also access the original source code as well as the entire set of generated images at https://github.com/jdespraz/deep_generative_networks

Table 2: Detailed generative network architecture (G).

LAYER	DIM	LAYER (CONT.)	DIM (CONT.)
Input Vector	1×3200	Batch Normalization	
Gaussian Noise		Upsampling	2×2
Locally Connected 1D	1×1	Convolution 2D	$128 \times 3 \times 3$
Reshape	$128 \times 5 \times 5$	Batch Normalization	
Upsampling	2×2	Convolution 2D	$128 \times 3 \times 3$
Convolution 2D	$512 \times 2 \times 2$	Batch Normalization	
Batch Normalization		Upsampling	2×2
Convolution 2D	$512 \times 2 \times 2$	Convolution 2D	$128 \times 3 \times 3$
Batch Normalization		Batch Normalization	
Upsampling	2×2	Convolution 2D	$128 \times 3 \times 3$
Convolution 2D	$256 \times 3 \times 3$	Batch Normalization	
Batch Normalization		Upsampling	2×2
Convolution 2D	$256 \times 3 \times 3$	Convolution 2D	$64 \times 3 \times 3$
Batch Normalization		Batch Normalization	
Upsampling	2×2	Convolution 2D	$64 \times 3 \times 3$
Convolution 2D	$256 \times 3 \times 3$	Batch Normalization	
Batch Normalization		Convolution 2D	$3 \times 3 \times 3$
Convolution 2D	$256 \times 3 \times 3$	Batch Normalization	